# Inner Limiting Membrane Barriers to AAV-mediated Retinal Transduction From the Vitreous

Deniz Dalkara[1–3], Kathleen D Kolstad[3,4], Natalia Caporale[3–5], Meike Visel[3,4], Ryan R Klimczak[3,4], David V Schaffer[1–3] and John G Flannery[3,4]

*[1]Department of Chemical Engineering, The University of California at Berkeley, Berkeley, California, USA; [2]Department of Bioengineering, The University of California at Berkeley, Berkeley, California, USA; [3]The Helen Wills Neuroscience Institute, The University of California at Berkeley, Berkeley, California, USA; [4]Department of Molecular and Cellular Biology, The University of California at Berkeley, Berkeley, California, USA; [5]Division of Neurobiology, University of California at Berkeley, Berkeley, California, USA*

Adeno-associated viral gene therapy has shown great promise in treating retinal disorders, with three promising clinical trials in progress. Numerous adeno-associated virus (AAV) serotypes can infect various cells of the retina when administered subretinally, but the retinal detachment accompanying this injection induces changes that negatively impact the microenvironment and survival of retinal neurons. Intravitreal administration could circumvent this problem, but only AAV2 can infect retinal cells from the vitreous, and transduction is limited to the inner retina. We therefore sought to investigate and reduce barriers to transduction from the vitreous. We fluorescently labeled several AAV serotype capsids and followed their retinal distribution after intravitreal injection. AAV2, 8, and 9 accumulate at the vitreoretinal junction. AAV1 and 5 show no accumulation, indicating a lack of appropriate receptors at the inner limiting membrane (ILM). Importantly, mild digestion of the ILM with a nonspecific protease enabled substantially enhanced transduction of multiple retinal cell types from the vitreous, with AAV5 mediating particularly remarkable expression in all retinal layers. This protease treatment has no effect on retinal function as shown by electroretinogram (ERG) and visual cortex cell population responses. These findings may help avoid limitations, risks, and damage associated with subretinal injections currently necessary for clinical gene therapy.

*Received 13 March 2009; accepted 13 July 2009; published online 11 August 2009. doi:10.1038/mt.2009.181*

## INTRODUCTION

Adeno-associated virus (AAV) has become the most promising ocular gene delivery vehicle over the past 10 years.[1–3] Its low immunogenicity, ability to infect the majority of retinal cells, and long-term transgene expression following a single treatment make the virus a very efficient gene delivery vector.[4] AAV is a nonpathogenic virus composed of a 4.7-kb single-stranded DNA genome enclosed within a 25-nm capsid.[5] In recombinant vectors, genes encoding replication (*rep*) and capsid (*cap*) proteins from the wild-type AAV genome are replaced by a promoter and therapeutic transgene cassette flanked by the AAV inverted terminal repeats that are required for packaging and replication. To date, hundreds of AAV variants have been identified,[6,7] and their tissue tropism and transduction efficiency are controlled by the capsid, which mediates initial receptor attachment, cellular entry, and trafficking mechanisms and thereby determines selectivity for particular cells or tissues. In particular, receptor-binding specificity is a key determinant of viral tropism. Specific glycan motifs have been identified as primary receptors for some AAV serotypes, and AAV2 uses heparan sulfate for cell recognition and entry whereas AAV1 and AAV5 bind to glycans with a terminal sialic acid.[8] In addition, AAV2, 8, and 9 bind to the 37/67-kDa laminin receptor,[9] likely as their secondary receptor.

AAV is particularly promising for gene therapy in the retina,[1–3] where mutations in genes expressed in photoreceptors and retinal pigment epithelia (RPEs) comprise the great majority of defects underlying inherited blindness. Because AAV is unable to reach these cells via intravitreal administration, the subretinal route of delivery is necessary. However, subretinal administration of AAV requires the surgeon to perform a vitrectomy, *i.e.*, create a needle hole through the retina (retinotomy) and detach the photoreceptors from the RPE with the injection of fluid. This retinal detachment causes series of macromolecular and structural modifications that are damaging to visual processing.[10] Also, in most retinal diseases, the degeneration is not uniform across the retina,[11–13] making identification of where to introduce the subretinal "bleb" difficult. Furthermore, the degenerating retina is often extremely fragile and poses a high risk of creating a retinal tear or macular hole.[14] Thus, in clinical settings it would be advantageous to introduce AAV vectors capable of outer retinal transduction from the vitreous.

It has been shown that after intravitreal injection, the AAV transduction profile of retinal cells differs significantly between neonatal and adult rats.[15] Injection of AAV2 at P0 results in photoreceptor, amacrine, and bipolar cell transduction, whereas the vast majority of transduced cells in adults are retinal ganglion

***Correspondence:*** *Deniz Dalkara, University of California at Berkeley, 132 Barker Hall, Berkeley, California 94720-3190, USA. E-mail: ddm@berkeley.edu*

cells (RGCs).[15] The inner limiting membrane (ILM)—a basement membrane that contains 10 distinct extracellular matrix proteins[16] and histologically defines the border between the retina and the vitreous humor[17]—may pose a barrier for penetration of AAV into the retina from the vitreous in adults, whereas a less-differentiated ILM or increased extracellular space may results in fewer barriers in the developing retina. Importantly, the ILM is essential for normal eye development;[18,19] however, it is dispensable in adults, and its removal is considered beneficial for patients undergoing macular hole surgery.[20]

We have investigated the localization and retinal transgene expression profile of five relevant AAV serotypes following intravitreal administration. In addition, we identified the ILM as a barrier to AAV-mediated retinal transduction by digesting it with Pronase E, a group of proteolytic enzymes from *Streptomyces griseus* previously shown to digest monkey ILM.[21] Specifically, coadministration of Pronase and AAV into the vitreous resulted in high-efficiency transduction of several retinal cell types, including photoreceptors and RPE. We anticipate this finding may greatly enhance AAV-mediated retinal gene therapy with intravitreal administration.

## RESULTS

### Labeling and characterization of AAV serotypes 1, 2, 5, 8, and 9

To assess the localization of viral particles in the retina after intravitreal injection, we labeled each AAV serotype by covalently linking a Cy3 amine–reactive dye to lysine residues exposed on the viral capsid surface.[22] Labeled virus was incubated with 293T cells to visualize particle localization before proceeding with *in vivo* studies (**Supplementary Figure S1a–c,g,h**). To confirm that fluorescent signal observed at the cell surface and in endosomal/lysosomal compartments was associated with intact viral particles, we employed immunocytochemistry. Antibodies against AAV1, 2, and 5 colocalized with the Cy3 dye (**Supplementary Figure S1d–f**), confirming Cy3 labeling is an appropriate means of monitoring viral dispersion in and among cells.

### Retinal penetration of Cy3-labeled viral particles following intravitreal injection

Localization of the different AAV serotypes after intravitreal injection was assessed by visualization of direct fluorescence resulting from the labeled capsids (**Supplementary Figure S2b,e,h,k,m**) and by immunostaining the same cryosections with anti-AAV capsid antibodies when available (**Supplementary Figure S2c,f,i**). The cryosections of retinas treated with AAV1-Cy3 did not exhibit any significant fluorescence (**Supplementary Figure S2b,c**). AAV5-Cy3 showed only very localized signal in displaced ganglion cells. To confirm that these results were not due to the difficulty of visualizing the Cy3 capsid label over tissue autofluorescence, AAV5-Cy3 was injected subretinally, and robust fluorescence was observed in the RPE and photoreceptors at the region of injection (**Supplementary Figure S3**). Cy3-AAV2 and nine injected retinas showed viral accumulation at the vitreoretinal junction (**Supplementary Figure S2e,m**), as indicated by punctate fluorescence on the ILM, at the RGCs, on the nerve fibers associated with RGCs, and at the Müller cell endfeet. AAV8 could also be detected at the vitreoretinal junction, though to a lesser extent (**Supplementary Figure S2k**).

Although AAV2 and 9 showed strikingly similar localization patterns, only AAV2 resulted in green fluorescent protein (GFP) expression in the retina 1 month after intravitreal injection (**Supplementary Figure S4**), consistent with prior reports with AAV2.

### Mild digestion of the ILM with Pronase E, a nonspecific protease

The localization of AAV2 and AAV9 at the vitreoretinal junction, where the ILM separates the vitreous from the retina, suggests that this anatomical feature may play a major role in initial viral attachment and subsequent penetration into the retina. It had been shown by Heegaard *et al.* that various enzymes can be used to disrupt the macaque monkey ILM.[21] After testing multiple glycosaminoglycases and proteases, the nonspecific protease, Pronase E, was shown to be the most successful agent in digesting the ILM. Pronase is a mixture of at least 10 proteases, including serine-type proteases, zinc endopeptidases, zinc leucine aminopeptidases, and a zinc carboxypeptidase.[23] We hypothesized that using Pronase E would disrupt the ILM, thereby enabling vector access to receptor-binding sites and potential cells that were previously unavailable to viral serotypes such as AAV1 and AAV5.

AAV is resistant to digestion by enzymes such as trypsin,[24] but we first confirmed that the AAV serotypes we used are also resistant to Pronase by performing *in vitro* tests. AAV was incubated with 0.01 and 0.05% Pronase E at 37 °C overnight, and DNase-resistant viral genomes were then quantified by quantitative PCR. We found that Pronase treatment did not degrade the viral capsid

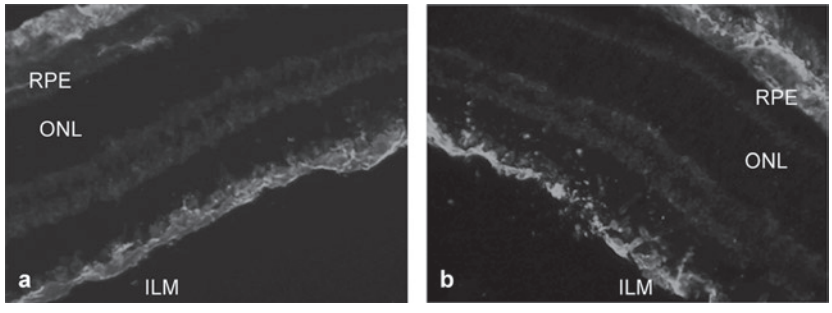


**Figure 1 Morphological effects of Pronase E on the inner limiting membrane (ILM).** (**a**) Untreated retina stained with anti-laminin antibody shows immunoreactivity at the ILM and at the choroid, whereas (**b**) laminin immunolabeling after treatment with 0.01% Pronase E exhibits a disintegrated ILM structure. ONL, outer nuclear layer; RPE, retinal pigment epithelium.

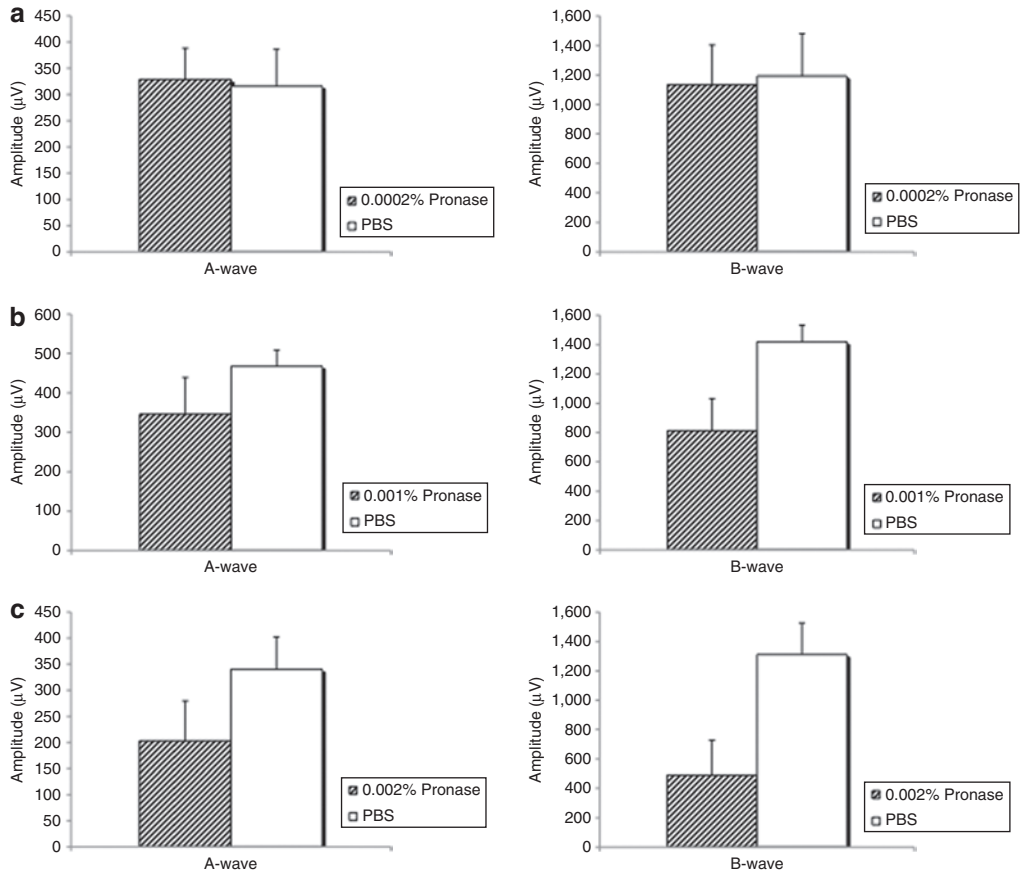


**Figure 2 The electroretinogram of animals injected with 0.0002% ($n$ = 8), 0.001% ($n$ = 6), and 0.002% ($n$ = 8) Pronase E was analyzed to assess toxicity of mild enzymatic cleavage of the inner limiting membrane (ILM).** Each animal was injected with the enzyme in the vitreous of one eye and phosphate-buffered saline (PBS) in the contralateral eye. Pronase E concentrations are (**a**) 0.0002%, (**b**) 0.001%, and (**c**) 0.002%. Pronase E injection exhibited no significant change in A- or B-wave amplitude compared to control PBS-injected eyes. Statistical differences between Pronase E and PBS-injected eyes were calculated by Student's *t*-test.

at the concentrations relevant for intraocular use (data not shown). Therefore, enzyme was mixed with AAV prior to all intravitreal injections to obviate the need for multiple injections into the same eye. As a control, virus was injected into the contralateral eye without the enzyme. Various doses of Pronase were used to permeabilize the ILM (0.01, 0.005, 0.001, and 0.0002% total) and revealed that enzyme levels were very important. At high doses, the disruptive effect of the enzyme on the ILM could be readily visualized by anti-laminin immunohistochemistry on cryosections of treated retinas (**Figure 1**). Interestingly, we have also observed some changes in the Pronase-treated ILM using transmission electron microscopy (**Supplementary Figure S5**), where retinas treated with Pronase showed a reduction in loose collagen fibrils and the appearance of dark aggregates along the ILM, which we hypothesize to be degraded proteins that have aggregated after enzymatic digestion. In contrast, at lower doses (≤0.001%) the effect of the enzyme on laminin immunohistochemistry was not pronounced.

We next analyzed whether these morphological changes corresponded to retinal functional changes and found that Pronase doses of ≤0.0002% did not alter electroretinograms (ERG) compared to the untreated eye (**Figure 2a**). Dosages >0.0002% are deleterious to the retina, as shown by a reduction in ERG A-wave and B-wave amplitudes (**Figure 2b,c**). As Pronase E is a nonselective protease, once it had disrupted the ILM, it likely perturbed the underlying nerve fiber layer and RGCs, which are essential components for vision. However, considering that only radial currents, and not RGC activity, are reflected in the ERG, we also

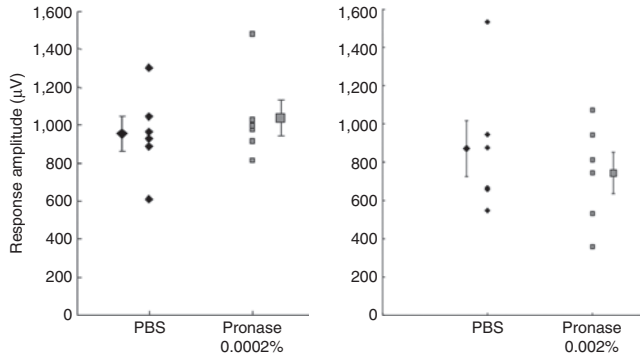


**Figure 3 Peak amplitude of visually evoked potentials in response to full-field stimulation of eyes injected with phosphate-buffered saline (PBS) (diamonds) or Pronase (squares) at the low dose, $n$ = 6, and high dose, $n$ = 6.** Recordings were performed on the contralateral visual cortex. Means for each data set are shown laterally displaced. Error bars indicate SEM. The two data sets for each dose were not significantly different ($n$ = 6, $P$ > 0.6, Wilcoxon signed-rank test).

recorded local field potential responses in V1 in animals treated with Pronase. These animals were only treated with enzyme in one eye, allowing the contralateral eye visual input to serve as an internal control. Interestingly, our data show that visually evoked potentials are more robust to enzymatic treatment compared to ERGs (**Figure 3**). A reduction was observed only at the highest concentration (**Figure 3**, right panel), yet this was not statistically significant ($n = 4$ out of 6). It is thus likely that the cortex is compensating for the reduction in signal.

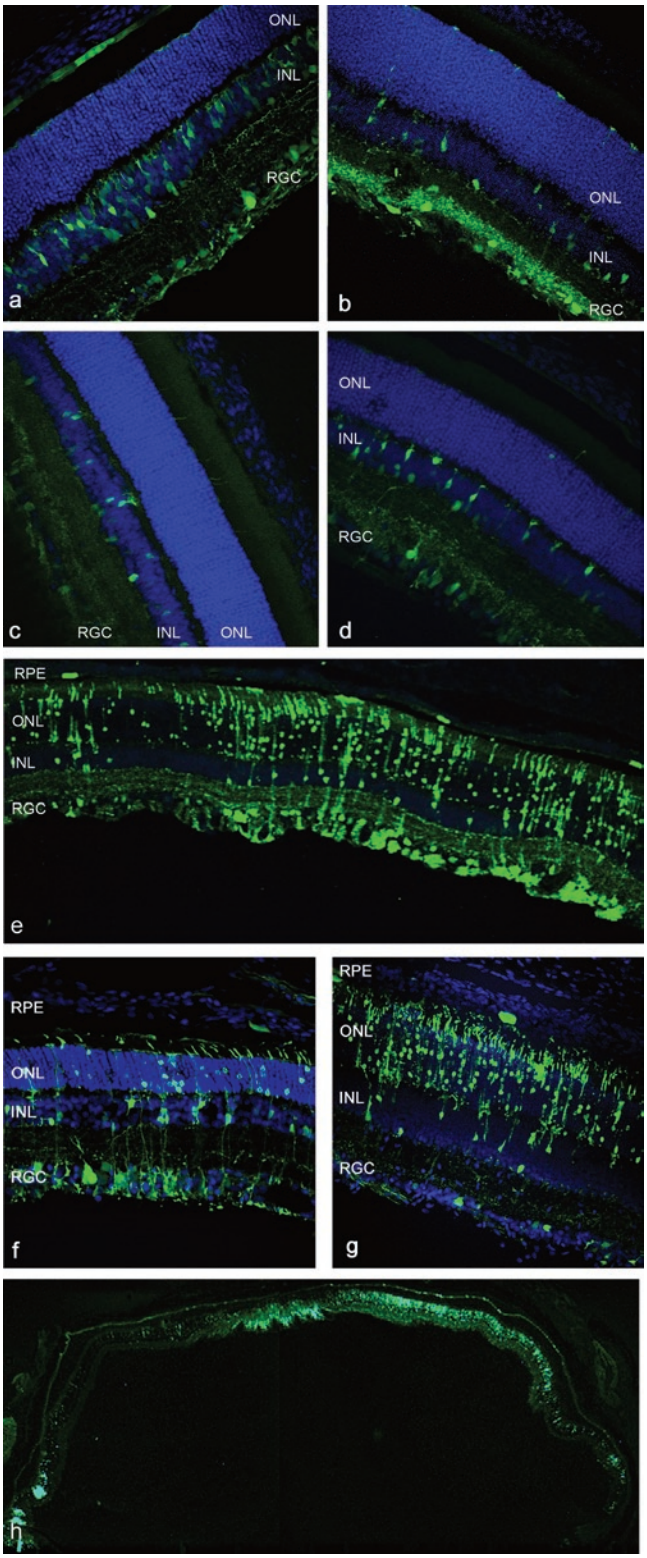


## GFP expression following AAV/Pronase E co-injection

All AAV serotypes injected intravitreally with Pronase (0.0002%) showed robust GFP expression in various cell types throughout the retina 3 weeks after injection (**Figure 4a–d**). In stark contrast, when AAV alone was injected intravitreally, only AAV2 led to gene expression in the inner retina, consistent with prior reports.[25] The strongest transduction was achieved with Pronase and AAV5 (**Figure 4e–h**), which mediated strong GFP expression in RGCs, Müller cells, photoreceptors, and RPE. The proportion of cells transduced varied throughout the extent of the retina (**Figure 4f–h**), potentially due to nonhomogeneous diffusion of the enzyme through the vitreous and a resulting higher concentration of the enzyme at the site of injection.

## DISCUSSION

AAV vectors traverse a complex pathway during the process of gene delivery. At the cellular level, viral binding to cell surface receptors, internalization, nuclear accumulation, capsid uncoating, and single- to double-stranded genome conversion can all represent barriers to gene transfer.[26,27] For *in vivo* delivery, however, the virus–host interaction begins at the site of administration, and the virus needs to bypass extracellular barriers such as basal membranes before reaching the target tissue and cells.

The tropism of AAV serotypes 1 through 9 has previously been studied in the retina.[28,29] Following subretinal delivery, AAV serotypes 1 and 4 primarily infect and mediate expression in RPE cells;[29,30] AAV2, 5, 7, 8, and 9 transduce RPE and photoreceptors;[28] and AAV8 and 9 also infect Müller glia. Interestingly, AAV5, 7, 8, and 9 also exhibit more efficient transduction and faster transgene expression than type 2 after subretinal injection. However, only AAV2 has been found to efficiently transduce the inner retina after intravitreal injection,[25] indicating that the vitreoretinal junction represents a tissue barrier to AAV gene delivery. Studies showing that physically larger viruses like Pseudorabies Virus are capable of RGC transduction from the vitreous[31] seem to indicate that the nature or this barrier is not diffusional or purely physical. In rodents, this feature of the retina is relatively thin and homogeneous; however, in larger animals such as dogs and monkeys, the ILM is significantly thicker and varies in thickness from one region of the retina to the other. This may have important consequences for translational studies relying on the intravitreal delivery of AAV.

In this study, we investigated and sought to overcome this barrier. After fluorescently labeling several relevant AAV serotype

**Figure 4 Green fluorescent protein (GFP) expression in cryosections of rat retina after intravitreal delivery of $10^{11}$ vector genomes of adeno-associated virus (AAV) vectors carrying smCBA.hGFP in the presence of 0.0002% Pronase, 3 weeks after injection.** Nuclei are stained with 4′,6-diamidino-2-phenylindole, shown in blue. (**a**) AAV1, (**b**) AAV2, (**c**) AAV8, (**d**) AAV9, and (**e**–**h**) AAV5. A representative area shows robust GFP fluorescence in all retinal layers in **e**. The proportion of transduced cells shows variability from one part to the other ($n = 6$) with strong expression in retinal ganglion cells (RGCs) and Müller cells in **f** and predominantly photoreceptors with weaker RGC with some expression in the RPE in **g**. An entire cryoslice is shown in **h**.

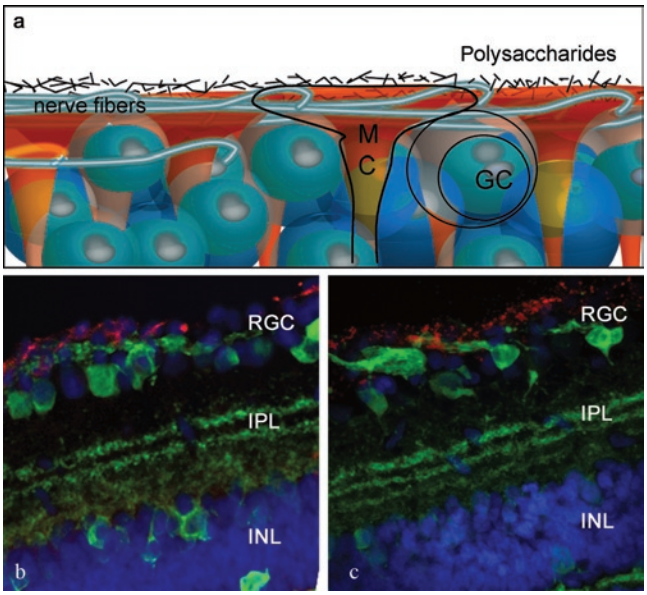


**Figure 5 AAV particle localization at the vitreoretinal junction.** (**a**) Schematic representation of the overlapping structures of the vitreoretinal junction. (**b**) Confocal images of AAV2-Cy3 and (**c**) AAV9-Cy3 accumulation at the vitreoretinal junction (red). The cryosections are counterstained with an antibody against calbindin (green), which labels the retinal neurons.

capsids, we visualized their localization in retinal tissue upon intravitreal injection. Serotypes 2, 8, and 9 were able to find attachment sites at the ILM and accumulate to various degrees at the vitreoretinal junction, and AAV2 and 9 in particular exhibited very similar localization patterns. However, the highly interdigitated nature of the components of the vitreoretinal junction (**Figure 5**) prevented us from clearly identifying the specific sites where viral particles had bounded and accumulated. AAV8 showed a weaker fluorescent signal at the ILM, indicating less robust attachment. It has been shown that the laminin receptor is involved in viral transduction by all three serotypes and could thus partially account for the attachment observed at the ILM, as laminin receptors are abundant at the vitreoretinal junction, the Müller cell endfeet, and RGCs.[32] In addition, AAV2 binds to heparan sulfate proteoglycan, also present at the ILM.[33] This binding may assist in viral accumulation at the ILM and thereby contributes to the intravitreal permissivity of this serotype. Interestingly, AAV2 and 9 seemed to show very similar fluorescent localization and signal intensity, yet AAV9 leads to no detectable expression after intravitreal injection (**Supplementary Figure S4**). Cell surface and intracellular trafficking barriers are likely to be responsible for this difference. A recent discovery shows that phosphorylation of surface-exposed capsid tyrosines target the AAV viral particles for ubiquitination and proteasome-mediated degradation, and mutations of these tyrosine residues lead to substantially increased vector transduction.[34] This finding has been used successfully to manipulate AAV retinal transduction profiles, and mutant AAV2, 8, and 9 displayed strong and widespread transgene expression in the inner retina after intravitreal delivery compared to their wild-type counterparts.[35] This finding, together with our localization results, clearly indicates that AAV serotypes 2, 8, and 9 are all able to bind to the vitreoretinal junction, but subsequent cellular barriers limit the transduction of inner retinal cells by AAV8 and 9.

In contrast to AAV2, 8, and 9, we find that AAV serotypes 1 and 5 are unable to find attachment sites at the vitreoretinal junction. It is known that both serotypes depend on sialic acid[36] for initial binding and that this monosaccharide is absent at the ILM.[37] Disruption of the ILM, a dispensable structure for the adult retina, using a nonspecific protease apparently resolves the access barrier to retinal transduction by sialic acid–dependent AAV serotypes 1 and 5.[8] In particular, our results show that intravitreal injection of AAV5 in combination with Pronase E leads to robust gene expression in various cells of the retina, including the RPE and photoreceptors. To our knowledge, this is the first time RPE transduction has been achieved by an intravitreally injected AAV vector. Interestingly, AAV5 is apparently the only serotype to date that is capable of packaging genomes larger than 4,700 nucleotides;[38] therefore, ILM digestion in conjunction with AAV5 delivery may allow for targeting of outer retinal cells without the need for subretinal injection and offers the capacity to deliver large genes to these cells.[38] Finally, a cell-specific promoter can be used to limit and control the levels of transgene expression in a cell type of choice.

Collectively, our data point to the importance of both extracellular and intracellular determinants of viral transduction in the retina. For intravitreal injections, viral binding and accumulation at an intact ILM may be necessary for the virus to access and infect the retina. By contrast, viral particles that lack binding sites at the ILM do not undergo concentration at this site, remain diffuse within the vitreous humor, and do not lead to gene expression. The ILM thus represents an important barrier to retinal gene delivery from the vitreous.

## MATERIALS AND METHODS

***Generation of rAAV vectors.*** AAV vectors containing sm.CBA promoter (which has the shortened hybrid chicken β–actin/rabbit β–globin intron) followed by enhanced GFP were produced by plasmid cotransfection into 293 cells.[39] The resulting clarified cell lysate was subjected to iodixanol density gradient purification, and the interface between 54 and 40% iodixanol fraction, along with the lower three-quarters of the 40% iodixanol fraction, was extracted after ultracentrifugation and diluted with an equal volume of phosphate-buffered saline (PBS) with 0.001% Tween-20. An Amicon Ultra-15 Centrifugal Filter Unit was preincubated with 5% Tween in PBS for 20 minutes, then washed once with PBS + 0.001% Tween. The diluted iodixanol fractions were loaded onto the centrifugal buffer exchange unit and spun until 250 µl of concentrated vector remained. Fifteen milliliters of sterile PBS + 0.001% Tween was added, and the concentration step was repeated three times with fresh sterile PBS + 0.001% Tween. A final viral concentrate of ~200 µl, devoid of iodixanol, was ultimately obtained. The vector was then titered for DNase-resistant vector genomes by quantitative PCR using diluted plasmid DNA as a standard. Finally, the purity of the vector was validated by silver-stained sodium dodecyl sulfate–polyacrylamide gel electrophoresis.

***Cy3 labeling of rAAV vectors.*** Purified and concentrated rAAV was labeled as previously described.[22] Briefly, amine-reactive Cy3 dye (GE Healthcare Biosciences, Uppsala, Sweden) was resuspended in a 0.2 mol/l $NaCO_3$/$NaHCO_3$ buffer at pH 9.3. Viral stock was mixed at a ratio of 1:1 with the dye suspension to a total volume of 400 µl. The reaction was allowed to take place for 2 hours at room temperature and quenched by the addition of 4 µl of 1 mol/l Tris–HCl at pH 8.0. Buffer exchange and concentration were then conducted using Amicon Ultra-5 Centrifugal Filter Units (Millipore, Billerica, MA).

***Intraocular administration routes.*** Adult wild-type Sprague-Dawley rats were used for all studies, and animal procedures were conducted according to the Association for Research in Vision and Ophthalmology statement for the use of animals and the National Institutes of Health guidelines for the use of laboratory animals, as approved by the Office of Laboratory Animal Care at the University of California at Berkeley. Before vector administration, rats were anesthetized with ketamine (72 mg/kg) and xylazine (64 mg/kg) by intraperitoneal injection. An ultrafine 30 1/2-gauge disposable needle was passed through the sclera, at the equator and next to the limbus, into the vitreous cavity. Injections were made with direct observation of the needle in the center of the vitreous cavity. The total volume delivered was 5 µl, containing 2–5 × $10^{12}$ vg/ml of AAV-Cy3. In addition, where indicated, 5 × $10^{12}$ vg/ml of AAV encoding enhanced GFP driven by the ubiquitous chicken β–actin promoter was mixed at a ratio of 4:1 with 0.001% Pronase E and injected.

***Fundus photography.*** *In vivo* retinal imaging was performed 2–4 weeks after injections with a fundus camera (RetCam II; Clarity Medical Systems, Pleasanton, CA) equipped with a wide angle 130° retinopathy of prematurity lens to monitor enhanced GFP expression in live, anesthetized rats. Pupils were dilated before imaging with tropicamide (1%).

***Electroretinography.*** Sprague-Dawley rats were injected with 5 µl of AAV5 encoding enhanced GFP mixed at a ratio of 4:1 with 0.0002% Pronase E in the vitreous of one eye and 5 µl of PBS in the contralateral eye, $n = 8$. This was repeated with the middle-dose (0.001%, final concentration, $n = 6$) and high-dose (0.002%, final concentration, $n = 8$) Pronase E concentrations. One-week postinjection, animals were dark-adapted for 4 hours and anesthetized, and their pupils were then dilated. Animals were placed on a heating pad, and contact lenses were positioned on the cornea. Reference electrodes were inserted subcutaneously in the cheeks, and a ground electrode was inserted in the tail. ERGs were recorded (Espion ERG system; Diagnosys, Littleton, MA) in response to seven light flash intensities from 0.0001 to 3.16 cd-s/$m^2$ presented in series of three. Light flash intensity and timing were elicited from a computer-controlled Ganzfeld flash unit. Data were analyzed with MatLab (v7.7; The MathWorks, Natick, MA). After correction for oscillatory potentials, scotopic A-wave values were measured from the baseline to the minimum ERG peak whereas scotopic B-waves were measured from the minimum to maximum ERG peaks. Statistical differences between Pronase E and PBS-injected eyes were calculated using paired Student's *t*-test.

***Cryosections.*** Two to four weeks after vector injection, rats were humanely euthanized, the eyes were enucleated, a hole was made in the cornea, and tissue was fixed with 10% neutral buffered formalin for 2–3 hours. The cornea and lens were removed. The eyecups were washed in PBS followed by 30% sucrose in PBS overnight. Eyes were then embedded in optimal cutting temperature embedding compound (Miles Diagnostics, Elkhart, IN) and oriented for 5–10-µm thick transverse retinal sections.

***Immunolabeling and histological analysis.*** Tissue sections were rehydrated in PBS for 5 minutes followed by incubation in a blocking solution of 1% bovine serum albumin, 0.5% Triton X-100, and 2% normal donkey serum in PBS for 2–3 hours. Slides were incubated overnight at 4 °C with commercial mouse monoclonal antibodies against intact capsids of AAV1, 2, or 5 (American Research Products, Belmont, MA) at 1:100, rabbit monoclonal antibody raised against the GFP (Invitrogen, Carlsbad, CA) at 1:400, or in anti-laminin antibody (L9393; Sigma, St Louis, MO) at 1:100 in blocking solution. The sections were then incubated with Alexa 488–conjugated secondary anti-rabbit antibody (Molecular Probes, Grand Island, NY) at 1:1,000 in blocking solution for 2 hours at room temperature. The results were analyzed by fluorescence microscopy using an Axiophot microscope (Zeiss, Thornwood, NY) equipped with X-Cite PC200 light source and QCapture Pro camera, or by confocal microscopy (LSM5; Carl Zeiss Microimaging, Thornwood, NY).

***Transmission electron microscopy.*** A generic processing protocol was used to prepare samples for transmission electron microscopy. Briefly, glutaraldehyde-fixed, osmocated retinas were treated with uranyl acetate at 4 °C overnight. Samples were then dehydrated with 35–100% water/acetone steps on ice. After Epon–Araldite resin infiltration, samples were left in a polymerization oven for 2 days. Sections of 70–100-nm thickness were cut from Epon–Araldite resin–embedded samples with a Reichert–Jung Ultra E microtome (Leica, Heerbrugg, Switzerland). They were collected on 0.6% Formvar-coated slot grids and poststained in 2% aqueous uranyl acetate and Reynold's lead citrate. Sections were imaged on a FEI Tecnai 12 TEM (FEI, Eindhoven, The Netherlands) with an UltraScan 1000 CCD camera (Gatan, Pleasanton, CA).

***Visually evoked potentials.*** A week prior to recordings, Sprague-Dawley rats were injected with 5 × $10^{13}$ vg/ml of AAV5 mixed at a ratio of 4:1 with 0.001% Pronase E ($n = 6$) or 5 × $10^{13}$ vg/ml of AAV5 mixed at a ratio of 4:1 with 0.01% Pronase E ($n = 6$) and injected in the vitreous of one eye and 5 µl of PBS in the contralateral eye. One week postinjection, animals were anesthetized using ketamine (72 mg/kg intraperitoneally) and xylazine (64 mg/kg intraperitoneally) and pupils dilated. Animals were restrained in a stereotaxic apparatus (David Kopf Instruments, Tujunga, CA), and body temperature was maintained at 36–37 °C via a heating blanket (Harvard Apparatus, Holliston, MA). Anesthesia was supplemented with 0.5–1% isoflurane as needed during the recordings. A small craniotomy and durotomy (~1 $mm^2$) were performed over the primary visual cortex (2–3 mm lateral to the midline, 1 mm anterior to λ). A glass micropipette (resistance ~0.5–3 MΩ) containing saline solution was lowered to 0.5–0.6 mm below the surface of the cortex and contralateral to the side of the stimulated eye. Visual stimulation consisted of 10-ms pulses of light (white LED, 1 cm from eye) presented at 0.2 Hz for 40–50 repeats. Sweeps were filtered at 2 kHz, sampled at 10 kHz by a 12-bit digital acquisition board (National Instruments, Austin, TX), and analyzed with custom software running in MatLab (The MathWorks).

## SUPPLEMENTARY MATERIAL

**Figure S1.** Cy3-labeled AAV particles at a MOI of $10^4$ were observed at the cell surface and in the endosomal/lysosomal compartments after a 20 min incubation with cells at 37 °C: a) AAV1-Cy3 b) AAV2-Cy3 c) AAV5-Cy3.

**Figure S2.** Localization of Cy3-labeled AAV particles in the retina of p30 rats.

**Figure S3.** Retinal cryosection showing spreading of Cy3-labeled AAV5 particles following subretinal injection.

**Figure S4.** Representative fundus image of eyes injected with a) AAV2.smCBA.hGFP and b) AAV9.smCBA.hGFP.

**Figure S5.** Comparative images of naïve and Pronase-treated retinas by TEM.

## ACKNOWLEDGMENTS

We acknowledge the National Institutes of Health grants EY016994-02 and 7PN2EY018241-03, and the Foundation Fighting Blindness for supporting this work. We thank Natalie Hoffman for her assistance with cryosectioning and Karen Guerin for her help in the preliminary experiments. We are also grateful to Jessie K Lee for excellent technical assistance in transmission electron microscopy and her expert input with the interpretation of the results. This work was done in Berkeley, CA, USA.

## REFERENCES

1. Mueller, C and Flotte, TR (2008). Clinical gene therapy using recombinant adeno-associated virus vectors. *Gene Ther* **15**: 858–863.
2. Lebherz, C, Maguire, A, Tang, W, Bennett, J and Wilson, JM (2008). Novel AAV serotypes for improved ocular gene transfer. *J Gene Med* **10**: 375–382.
3. Hauswirth, WW, Aleman, TS, Kaushal, S, Cideciyan, AV, Schwartz, SB, Wang, L *et al.* (2008). Treatment of leber congenital amaurosis due to RPE65 mutations by ocular subretinal injection of adeno-associated virus gene vector: short-term results of a phase I trial. *Hum Gene Ther* **19**: 979–990.

4. Büning, H, Perabo, L, Coutelle, O, Quadt-Humme, S and Hallek, M (2008). Recent developments in adeno-associated virus vector technology. *J Gene Med* **10**: 717–733.
5. Goncalves, MA (2005). Adeno-associated virus: from defective virus to effective vector. *Virol J* **2**: 43.
6. Gao, G, Vandenberghe, LH, Alvira, MR, Lu, Y, Calcedo, R, Zhou, X *et al.* (2004). Clades of Adeno-associated viruses are widely disseminated in human tissues. *J Virol* **78**: 6381–6388.
7. Wu, Z, Asokan, A and Samulski, RJ (2006). Adeno-associated virus serotypes: vector toolkit for human gene therapy. *Mol Ther* **14**: 316–327.
8. Wu, Z, Miller, E, Agbandje-McKenna, M and Samulski, RJ (2006). Alpha2,3 and alpha2,6 N-linked sialic acids facilitate efficient binding and transduction by adeno-associated virus types 1 and 6. *J Virol* **80**: 9093–9103.
9. Akache, B, Grimm, D, Pandey, K, Yant, SR, Xu, H and Kay, MA (2006). The 37/67-kilodalton laminin receptor is a receptor for adeno-associated virus serotypes 8, 2, 3, and 9. *J Virol* **80**: 9831–9836.
10. Fisher, SK, Lewis, GP, Linberg, KA and Verardo, MR (2005). Cellular remodeling in mammalian retina: results from studies of experimental retinal detachment. *Prog Retin Eye Res* **24**: 395–431.
11. Jacobson, SG, Aleman, TS, Cideciyan, AV, Roman, AJ, Sumaroka, A, Windsor, EA *et al.* (2009). Defining the residual vision in leber congenital amaurosis caused by RPE65 mutations. *Invest Ophthalmol Vis Sci* **50**: 2368–2375.
12. Jacobson, SG, Aleman, TS, Sumaroka, A, Cideciyan, AV, Roman, AJ, Windsor, EA *et al.* (2009). Disease boundaries in the retina of patients with Usher syndrome caused by MYO7A gene mutations. *Invest Ophthalmol Vis Sci* **50**: 1886–1894.
13. Jacobson, SG, Aleman, TS, Cideciyan, AV, Sumaroka, A, Schwartz, SB, Windsor, EA *et al.* (2005). Identifying photoreceptors in blind eyes caused by RPE65 mutations: prerequisite for human gene therapy success. *Proc Natl Acad Sci USA* **102**: 6177–6182.
14. Maguire, AM, Simonelli, F, Pierce, EA, Pugh, EN Jr., Mingozzi, F, Bennicelli, J *et al.* (2008). Safety and efficacy of gene transfer for Leber's congenital amaurosis. *N Engl J Med* **358**: 2240–2248.
15. Harvey, AR, Kamphuis, W, Eggers, R, Symons, NA, Blits, B, Niclou, S *et al.* (2002). Intravitreal injection of adeno-associated viral vectors results in the transduction of different types of retinal neurons in neonatal and adult rats: a comparison with lentiviral vectors. *Mol Cell Neurosci* **21**: 141–157.
16. Candiello, J, Balasubramani, M, Schreiber, EM, Cole, GJ, Mayer, U, Halfter, W *et al.* (2007). Biomechanical properties of native basement membranes. *FEBS J* **274**: 2897–2908.
17. Halfter, W, Dong, S, Dong, A, Eller, AW and Nischt, R (2008). Origin and turnover of ECM proteins from the inner limiting membrane and vitreous body. *Eye* **22**: 1207–1213.
18. Halfter, W (1998). Disruption of the retinal basal lamina during early embryonic development leads to a retraction of vitreal end feet, an increased number of ganglion cells, and aberrant axonal outgrowth. *J Comp Neurol* **397**: 89–104.
19. Semina, EV, Bosenko, DV, Zinkevich, NC, Soules, KA, Hyde, DR, Vihtelic, TS *et al.* (2006). Mutations in laminin alpha 1 result in complex, lens-independent ocular phenotypes in zebrafish. *Dev Biol* **299**: 63–77.
20. Mester, V and Kuhn, F (2000). Internal limiting membrane removal in the management of full-thickness macular holes. *Am J Ophthalmol* **129**: 769–777.
21. Heegaard, S, Jensen, OA and Prause, JU (1986). Structure and composition of the inner limiting membrane of the retina. SEM on frozen resin-cracked and enzyme-digested retinas of Macaca mulatta. *Graefes Arch Clin Exp Ophthalmol* **224**: 355–360.
22. Bartlett, JS, Wilcher, R and Samulski, RJ (2000). Infectious entry pathway of adeno-associated virus and adeno-associated virus vectors. *J Virol* **74**: 2777–2785.
23. Jurásek, J, Johnson, P, Olafson, RW and Smillie, LB (1971). An improved fractionation system for pronase on CM-sephadex. *Can J Biochem* **49**: 1195–1201.
24. Van Vliet, K, Blouin, V, Agbandje-McKenna, M and Snyder, RO (2006). Proteolytic mapping of the adeno-associated virus capsid. *Mol Ther* **14**: 809–821.
25. Surace, EM and Auricchio, A (2008). Versatility of AAV vectors for retinal gene transfer. *Vision Res* **48**: 353–359.
26. McCarty, DM (2008). Self-complementary AAV vectors; advances and applications. *Mol Ther* **16**: 1648–1656.
27. Schultz, BR and Chamberlain, JS (2008). Recombinant adeno-associated virus transduction and integration. *Mol Ther* **16**: 1189–1199.
28. Allocca, M, Mussolino, C, Garcia-Hoyos, M, Sanges, D, Iodice, C, Petrillo, M *et al.* (2007). Novel adeno-associated virus serotypes efficiently transduce murine photoreceptors. *J Virol* **81**: 11372–11380.
29. Auricchio, A, Kobinger, G, Anand, V, Hildinger, M, O'Connor, E, Maguire, AM *et al.* (2001). Exchange of surface proteins impacts on viral vector cellular specificity and transduction characteristics: the retina as a model. *Hum Mol Genet* **10**: 3075–3081.
30. Weber, M, Rabinowitz, J, Provost, N, Conrath, H, Folliot, S, Briot, D *et al.* (2003). Recombinant adeno-associated virus serotype 4 mediates unique and exclusive long-term transduction of retinal pigmented epithelium in rat, dog, and nonhuman primate after subretinal delivery. *Mol Ther* **7**: 774–781.
31. Pickard, GE, Smeraski, CA, Tomlinson, CC, Banfield, BW, Kaufman, J, Wilcox, CL *et al.* (2002). Intravitreal injection of the attenuated pseudorabies virus PRV Bartha results in infection of the hamster suprachiasmatic nucleus only by retrograde transsynaptic transport via autonomic circuits. *J Neurosci* **22**: 2701–2710.
32. Chai, L and Morris, JE (1999). Heparan sulfate in the inner limiting membrane of embryonic chicken retina binds basic fibroblast growth factor to promote axonal outgrowth. *Exp Neurol* **160**: 175–185.
33. Chai, L and Morris, JE (1994). Distribution of heparan sulfate proteoglycans in embryonic chicken neural retina and isolated inner limiting membrane. *Curr Eye Res* **13**: 669–677.
34. Zhong, L, Li, B, Mah, CS, Govindasamy, L, Agbandje-McKenna, M, Cooper, M *et al.* (2008). Next generation of adeno-associated virus 2 vectors: point mutations in tyrosines lead to high-efficiency transduction at lower doses. *Proc Natl Acad Sci USA* **105**: 7827–7832.
35. Petrs-Silva, H, Dinculescu, A, Li, Q, Min, SH, Chiodo, V, Pang, JJ *et al.* (2009). High-efficiency transduction of the mouse retina by tyrosine-mutant AAV serotype vectors. *Mol Ther* **17**: 463–471.
36. Kaludov, N, Brown, KE, Walters, RW, Zabner, J and Chiorini, JA (2001). Adeno-associated virus serotype 4 (AAV4) and AAV5 both require sialic acid binding for hemagglutination and efficient transduction but differ in sialic acid linkage specificity. *J Virol* **75**: 6884–6893.
37. Cho, EY, Choi, HL and Chan, FL (2002). Expression pattern of glycoconjugates in rat retina as analysed by lectin histochemistry. *Histochem J* **34**: 589–600.
38. Allocca, M, Doria, M, Petrillo, M, Colella, P, Garcia-Hoyos, M, Gibbs, D *et al.* (2008). Serotype-dependent packaging of large genes in adeno-associated viral vectors results in effective gene delivery in mice. *J Clin Invest* **118**: 1955–1964.
39. Grieger, JC, Choi, VW and Samulski, RJ (2006). Production and characterization of adeno-associated viral vectors. *Nat Protoc* **1**: 1412–1428.